



Phase evolution, far-infrared spectra, and ultralow loss microwave dielectric ceramic of $\text{Zn}_2\text{Ge}_{1+x}\text{O}_{4+2x}$ ($-0.1 \leq x \leq 0.2$)

Changzhi Yin^{1,2} · Ying Tang^{1,2} · Junqi Chen^{1,2} · Chunchun Li^{1,2,3} · Liang Fang^{1,2,4} · Feihu Li^{1,2} · Yijun Huang^{1,2}

Received: 20 May 2019 / Accepted: 13 August 2019 / Published online: 31 August 2019
© Springer Science+Business Media, LLC, part of Springer Nature 2019

Abstract

A series of willemite based ceramics $\text{Zn}_2\text{Ge}_{1+x}\text{O}_{4+2x}$ with $-0.1 \leq x \leq 0.2$ were prepared by the solid-state reaction method. Influences of Ge nonstoichiometry on the crystal structure, densification, and microwave dielectric properties were evaluated in terms of X-ray diffraction, SEM, dielectric measurements and far-infrared spectra. Ge excess favored the formation of single-phase willemite but a high level of excess induced appearance of GeO_2 . In contrast, nominal composition and those with Ge deficiency comprised of ZnO and the willemite phase. Ge excess was found to be beneficial to the densification and dielectric properties optimization of $\text{Zn}_2\text{Ge}_{1+x}\text{O}_{4+2x}$. A composition with $x=0.1$ ($\text{Zn}_2\text{Ge}_{1.1}\text{O}_{4.2}$) exhibited the optimum microwave dielectric properties with a relative permittivity $\epsilon_r \sim 7.09$, a quality factor $Q \times f \sim 112,700$ GHz (at 14.48 GHz), and a temperature coefficient of resonance frequency $\tau_f \sim -51$ ppm/°C.

1 Introduction

Modern electronic components in wireless communication systems, such as dielectric resonators, filters, antennas, etc. rely on microwave dielectric materials which exhibit excellent dielectric performances at microwave or millimeter-wave frequency region. The recent progress in high-frequency data transmission (5G network) and the Internet of Things (IoT) has prompted the development of novel design methods and materials with prominent physical properties. Generally, there are three primary requirements that must be satisfied: applicable dielectric constant (ϵ_r), high quality factor (low dielectric loss, $Q=1/\tan\delta$), and near-zero temperature coefficient of resonant frequency (τ_f) [1–3]. It is

well known that the data transmission speed is in inverse proportion to the square root of ϵ_r . As a result, low ϵ_r is crucial for high-speed data transmission and is a benefit to minimize the cross-coupling with the conductors.

In the past several decades, some low- ϵ_r dielectric ceramics have been investigated, which is mainly focused on silicates [4, 5], germanates [6], phosphates [7], and vanadates [8, 9], etc. Among them, M_2SiO_4 ($\text{M}=\text{Zn}, \text{Mg}$) has attracted wide attention due to their low permittivity ($\epsilon_r \sim 6.6$ and 6.8) and high quality factor ($Q \times f \sim 219,000$ GHz and 270,000 GHz) [10–12]. But silicate ceramics need high sintering temperature up to 1350 °C to be densified because of the refractive nature of silicon dioxide. Olivine germanates are analogs to silicates but with relatively lower sintering temperature because of the low melting point of germanium dioxide (~ 1115 °C). Recently, microwave dielectric properties of Mg_2GeO_4 ceramics sintered at 1250 °C were reported with a low permittivity ($\epsilon_r \sim 6.76$), a quality factor ($Q \times f \sim 95,000$ GHz), and a temperature coefficient of resonant frequency ($\tau_f \sim -28.7$ ppm/°C) [13]. Moreover, Zn_2GeO_4 ceramics were reported to have promising microwave dielectric properties with $\epsilon_r \sim 6.87$, $Q \times f \sim 102,700$ GHz, and $\tau_f \sim -32.4$ ppm/°C [14]. But there is a controversy about the phase formation of Zn_2GeO_4 . Eoh et al. [15] reported that nominal starting composition Zn_2GeO_4 could not form a single phase but with ZnO secondary phase [12, 16]. ZnO-deficient ceramic $\text{Zn}_{1.9}\text{GeO}_{3.9}$, however, crystallized in a pure Zn_2GeO_4

✉ Ying Tang
tangyinggl001@aliyun.com

✉ Liang Fang
fangliangg1001@aliyun.com

¹ Guangxi Key Laboratory of Optical and Electronic Materials and Devices, Guilin University of Technology, Guilin 541004, China

² College of Material Science and Engineering, Guilin University of Technology, Guilin 541004, China

³ College of Information Science and Engineering, Guilin University of Technology, Guilin 541004, China

⁴ College of Materials and Chemical Engineering, Three Gorges University, Yichang 443002, China

phase with microwave dielectric properties of $\epsilon_r = 6.8$, $Q \times f = 49,000$ GHz, and $\tau_f = -16.7$ ppm/°C [17]. It is well known that the dielectric properties, especially the quality factor are sensitive to the second phases [2]. Thus, the existence of the ZnO phase in Zn_2GeO_4 would degrade the dielectric performances. As a result, with an attempt to verify the phase formation and to optimize the dielectric properties of Zn_2GeO_4 , slight Ge nonstoichiometry was designed and a series of $\text{Zn}_2\text{Ge}_{1+x}\text{O}_{4+2x}$ ($x = -0.1, -0.05, 0, 0.02, 0.05, 0.1, 0.15$ and 0.2) were prepared and their phase formation, sintering behavior, and microwave dielectric properties were studied.

2 Experimental

$\text{Zn}_2\text{Ge}_{1+x}\text{O}_{4+2x}$ ($-0.1 \leq x \leq 0.2$) ceramics were prepared by the solid-state reaction from high-purity oxides ZnO (99.99%, Guo-Yao Co. Ltd, China), GeO_2 (99.999%, Guo-Yao Co. Ltd, China). The raw materials were weighed stoichiometrically and mixed via ball milling with ZrO_2 balls in the nylon jar at a speed of 300 rpm for 6 h. After dried, the resultant mixed powders were calcined at 950 °C for 6 h. The calcined powders were re-milled, dried and added with 5 wt% PVA as the binder, then pressed into 10 mm-diameter and 6 mm-height disks under a uniaxial pressure of 80 MPa. The green samples were firstly fired to 550 °C for 4 h to remove the organic binder and then sintered over a temperature range of 980–1220 °C.

The phase purity was analyzed by an X-ray diffractometer (XRD; CuK α 1, 1.54059 Å, Model X' Pert PRO, PANalytical, Almelo, The Netherlands) and Raman spectrometer (DXR; Thermo Fisher Scientific, American). The surface microstructure was observed using a scanning electron microscopy (SEM, S4800, Hitachi, Tokyo, Japan). The bulk density was measured by Archimedes' method. The theoretical density of the two-phase system was calculated by the equation:

$$\rho_{\text{th}} = \frac{\omega_1 + \omega_2}{\omega_1/\rho_1 + \omega_2/\rho_2} \quad (1)$$

where ω_1 , ω_2 , and ρ_1 , ρ_2 are the mass fractions and theory density of Zn_2GeO_4 and the second phase (ZnO or GeO_2), respectively.

A network analyzer (N5230A, Agilent Co., Palo Alto, CA) connected with a temperature chamber (Delta 9039; Delta Design, San Diego, CA) was used to measure the microwave dielectric properties. The permittivity and $\tan \delta$ measured at 1 MHz by the bridge method using HP 4294A are provided for comparison. The τ_f value measured from 25 to 85 °C was calculated by an equation as follows:

$$\tau_f = \frac{f_2 - f_1}{f_1(T_2 - T_1)} \quad (2)$$

where f_1 and f_2 denote the resonant frequency at T_1 (25 °C) and T_2 (85 °C), respectively.

To obtain the intrinsic contributions to the dielectric properties, the room-temperature infrared reflectivity spectra were measured by a Bruker IFS 66v FT-IR spectrometer (Bruker Optics, Ettlingen, Germany). The data were analyzed using the classical harmonic oscillator model:

$$\epsilon^*(\omega) = \epsilon_\infty + \sum_{j=1}^n \frac{\omega_{pj}^2}{\omega_{oj}^2 - \omega^2 - j\gamma_j\omega} \quad (3)$$

$$R(\omega) = \left| \frac{1 - \sqrt{\epsilon^*(\omega)}}{1 + \sqrt{\epsilon^*(\omega)}} \right| \quad (4)$$

where the ϵ_∞ is the dielectric constant at optical frequency, $\epsilon^*(\omega)$ is complex permittivity, n is the number of transverse phonon modes, γ_j , ω_{oj} and ω_{pj} is the damping factor, the transverse frequency and plasma frequency of the j_{th} Lorentz oscillator, respectively.

3 Results and discussion

3.1 Crystal structure and microstructure characterizations

Figure 1 shows the room-temperature XRD patterns performed on the cracked powders of the sintered $\text{Zn}_2\text{Ge}_{1+x}\text{O}_{4+2x}$ ($-0.1 \leq x \leq 0.2$) samples at 1050 °C for 6 h. In the nominal composition with $x=0$, the main phase was confirmed as Zn_2GeO_4 (JCPDS No. 11-0687), whereas traceable diffraction peaks belonging to ZnO (JCPDS No. 36-1451) were also detected, which is consistent with Eoh's report [15]. Fortunately, the intensity of ZnO decreased obviously with slight Ge excess. It is notable that a single-phase region exists when $0 < x < 0.05$ with no evidence of any second phase(s) within the instrument resolution. In contrast, Ge deficiency favors the formation of ZnO characterized by increased peak intensity with decreasing Ge amount. These results demonstrate that slight Ge excess suppresses ZnO formation and is beneficial to phase formation of Zn_2GeO_4 but the excess magnitude is extremely limited to approximately 5 mol%, beyond which GeO_2 will remain and becomes more distinct as x value increases. A similar phenomenon was found in spinel-like ZnMn_2O_4 , in which single phase was formed by adjusting Zn/Mn ratios [18].

To further confirm the phase constitution and purity, Rietveld refinements were performed and the representative results for the $x = -0.05, 0, 0.02$, and 0.05 samples are shown in Fig. 2. Notably, a bi-phase refinement with Zn_2GeO_4 and ZnO as structural models was conducted to

Fig. 1 X-ray diffraction patterns of the calcined $Zn_2Ge_{1+x}O_{4+2x}$ powders at 1050 °C for 6 h

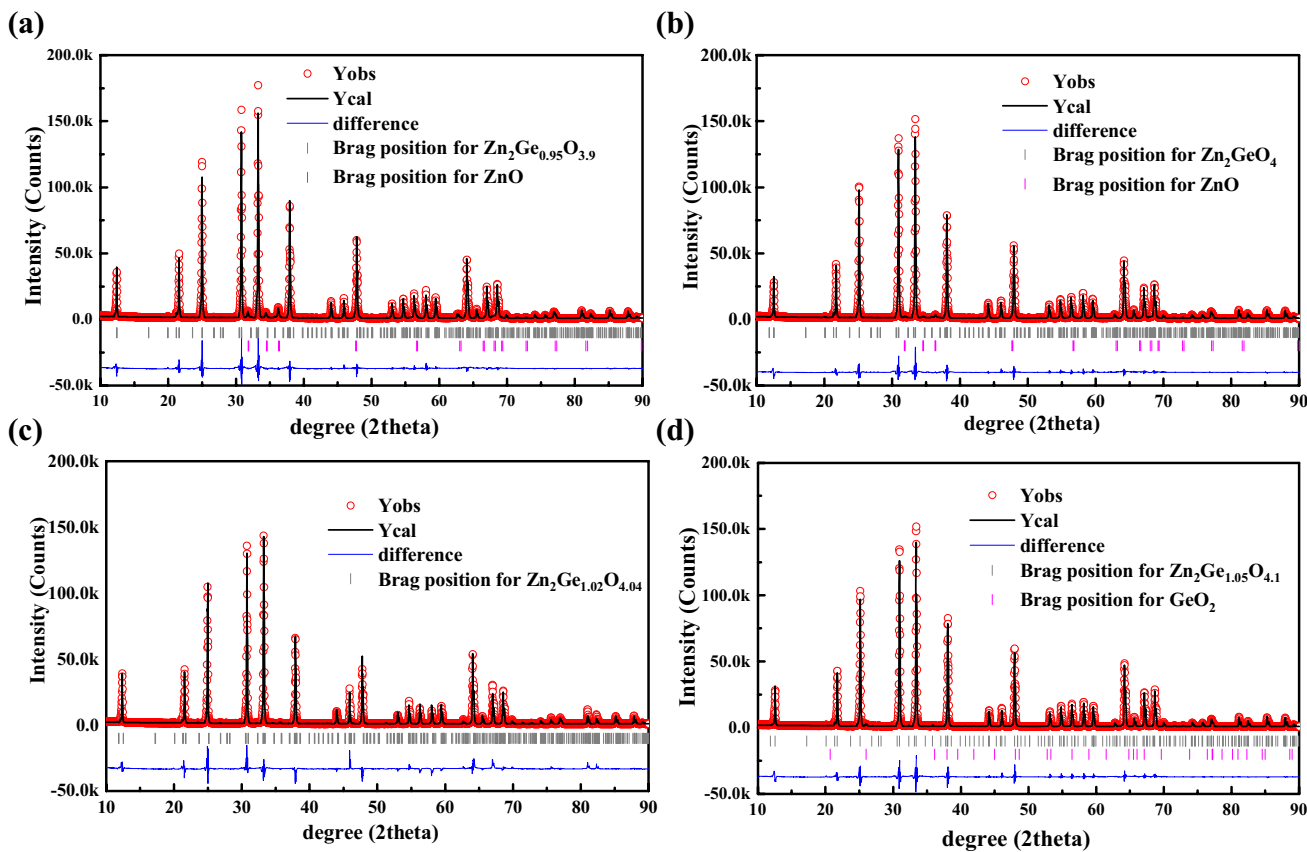
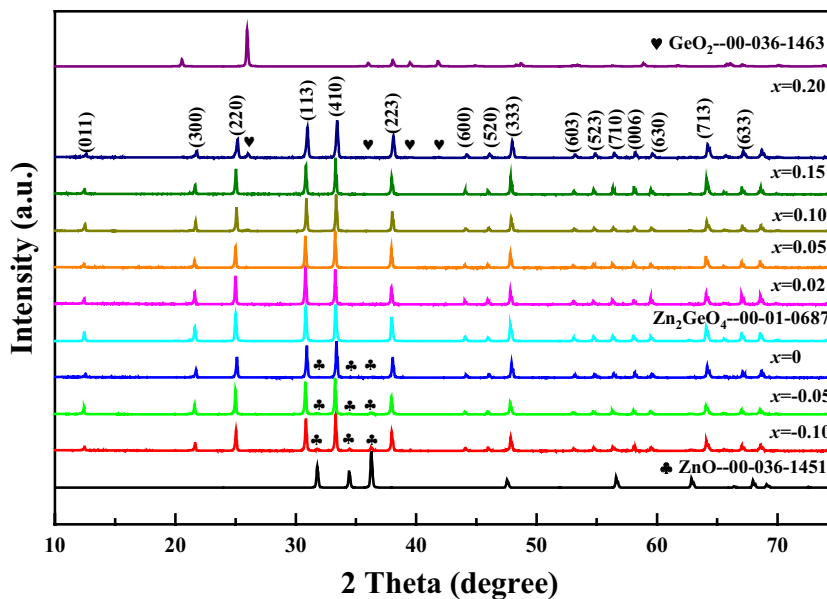


Fig. 2 Typical Rietveld refinement plots for $Zn_2Ge_{1+x}O_{4+2x}$ with **a** $x = -0.05$; **b** $x = 0$; **c** $x = 0.02$; **d** $x = 0.05$

the $x = -0.05$ and $x = 0$ samples, while Zn_2GeO_4 and GeO_2 for samples with $x = 0.05$. In contrast, the $x = 0.02$ sample could be well refined merely with Zn_2GeO_4 as a structural model. Table 1 gives the lattice parameters, residual factors,

phase volume fraction from the Rietveld refinement. For each composition, the good match between the observed and calculated profiles yields low residual factors, suggesting the validity and reliability of the refinement. In addition,

Table 1 Lattice parameters, residual factors, phase volume fraction of $\text{Zn}_2\text{Ge}_{1+x}\text{O}_{4+2x}$ ($x = -0.05, 0, 0.02, \text{ and } 0.05$)

x value	Phase	Phase fraction (%)	Lattice parameters (Å)		Volume (\AA^3)	R factors (%)		
			$a=b$	c		R_{wp}	R_p	R_{exp}
-0.05	Zn_2GeO_4 (R-3)	94.5	14.2328	9.5246	1670.9293	11.97	8.89	1.82
	ZnO (P6 ₃ mc)	5.5	3.2504	5.2071	47.6431			
0	Zn_2GeO_4 (R-3)	97.1	14.2374	9.5277	1672.5537	10.37	7.70	1.88
	ZnO (P6 ₃ mc)	2.9	3.2505	5.2081	47.6552			
0.02	Zn_2GeO_4 (R-3)	100	14.2379	9.5284	1672.7941	9.85	5.61	1.82
0.05	Zn_2GeO_4 (R-3)	99.1	14.2384	9.5292	1673.0521	11.85	8.71	1.91
	GeO_2 (P3 ₁ 21)	0.9	4.9868	5.6924	122.5942			

the magnitude of ZnO phase dropped clearly from 5.5% for $x = -0.05$ to 2.9% for $x = 0$, and finally vanished at $x = 0.02$, after which GeO_2 appeared as the secondary phase with a value of 0.9% at $x = 0.05$.

SEM images of the $\text{Zn}_2\text{Ge}_{1+x}\text{O}_{4+2x}$ ($-0.1 \leq x \leq 0.2$) ceramics sintered at their optimum temperatures are shown in Fig. 3. All compositions have dense microstructures characterized by closely packed grains and clearly distinguished grain boundaries except for the nominal Zn_2GeO_4 that exhibits visible pores. Obviously, the grain size gradually grew from 2–5 μm at $x = -0.1$ to 4–8 μm at $x = 0.1$. Additionally, a great change in grain morphology is observed from granular grains in the Ge-deficient samples to columnar ones in the Ge-rich samples. These results indicate that Ge excess facilitates densification and grain growth of Zn_2GeO_4 ceramics. The preferential growth of Zn_2GeO_4 has previously verified and is evident from the preferentially oriented columnar grains [19]. To determine the chemical composition of $\text{Zn}_2\text{Ge}_{1+x}\text{O}_{4+2x}$ ($-0.1 \leq x \leq 0.2$) ceramics, EDX results illustrated that the atomic ratio of Zn:Ge was 2:0.92 for $x = -0.1$ and 2:1.03 for $x = 0.05$, which is in good agreement with the stoichiometry. XRD results show that the main phase for both compositions is Zn_2GeO_4 irrespective of the Zn/Ge ratio. Especially, the $x = -0.1$ sample was a bi-phase with evident ZnO phase while $x = 0.05$ is Zn_2GeO_4 phase mixed with a small amount of GeO_2 . Therefore, their different microstructure might be related to the second phase. Compared to ZnO (~ 1975 °C), GeO_2 has a relatively low melting point (~ 1115 °C), acting as a sintering aid at elevated temperatures, which promotes grain growth in Ge-rich samples. It should be noted, however, it is difficult to distinguish the ZnO/ GeO_2 second phase in the SEM images.

3.2 Microwave dielectric properties

Figure 4a shows the bulk densities of all samples sintered at various temperatures from 980 to 1220 °C. With increasing sintering temperature, the density of all samples exhibited a similar variation trend, that is, the density increased to reach a maximum value and then decreased with further increase

in the sintering temperature. The sintering temperature, relative density, and bulk density are shown in Fig. 4b as a function of x value. The density decreased with x increasing from -0.1 to 0 whereas it increased with x increasing from 0.02 to 0.1. The high density of the samples with $x \leq 0$ is mainly owing to the high density of ZnO (5.606 g/cm³) while GeO_2 with a low density (4.228 g/cm³) is responsible for the relatively lower density when $x \geq 0.05$. It is noteworthy that the relative densities of all the samples were over 95%, which suggests that the as-sintered samples were suitable for the subsequent dielectric measurements.

The τ_f values of the $\text{Zn}_2\text{Ge}_{1+x}\text{O}_{4+2x}$ ceramics sintered at their relative optimum temperatures are shown in Fig. 4c, which fluctuates in the range of -45 to -52 ppm/°C. Figure 4d shows the relative permittivity (ϵ_r), quality factor ($Q \times f$), and loss tangent ($\tan\delta$) as a function of x value. It should be noted that the permittivity ϵ_r and $\tan\delta$ of the nominal and the Ge deficient Zn_2GeO_4 samples with $x = -0.1, -0.05$ and 0 cannot be obtained using the resonance method because of the adverse effects from the second phase ZnO. Instead, the values measured at 1 MHz by the bridge method using HP 4294A were provided for comparison. The relative permittivity increased from 6.73 to 7.09 with x from -0.1 to 0.1 and then decreased at $x = 0.15$. The increasing permittivity is believed to be mainly due to the enhanced density and partly attributed to the higher permittivity of ZnO ($\epsilon_r = 7.5$) [20] compared to Zn_2GeO_4 ($\epsilon_r = 6.87$) [14].

The dielectric loss tangent ($\tan\delta$) measured at 1 MHz for compositions with $-0.1 \leq x \leq 0$ are much higher compared to those values at microwave frequency. This is due to the different measurement frequencies and the adverse effects from the second phase ZnO. The $Q \times f$ versus x values presented a similar behavior to that of permittivity at $0.02 \leq x \leq 0.2$, reaching a peak value of 112,700 GHz at $x = 0.1$ and then decreased to 94,900 GHz at $x = 0.15$. The variation in $Q \times f$ value reflects the competitive effects of GeO_2 excess. Appropriate GeO_2 excess addition was proved to improve the densification and facilitate grain preferential growth [19], which was beneficial to bring down the extrinsic contributions to dielectric losses, such

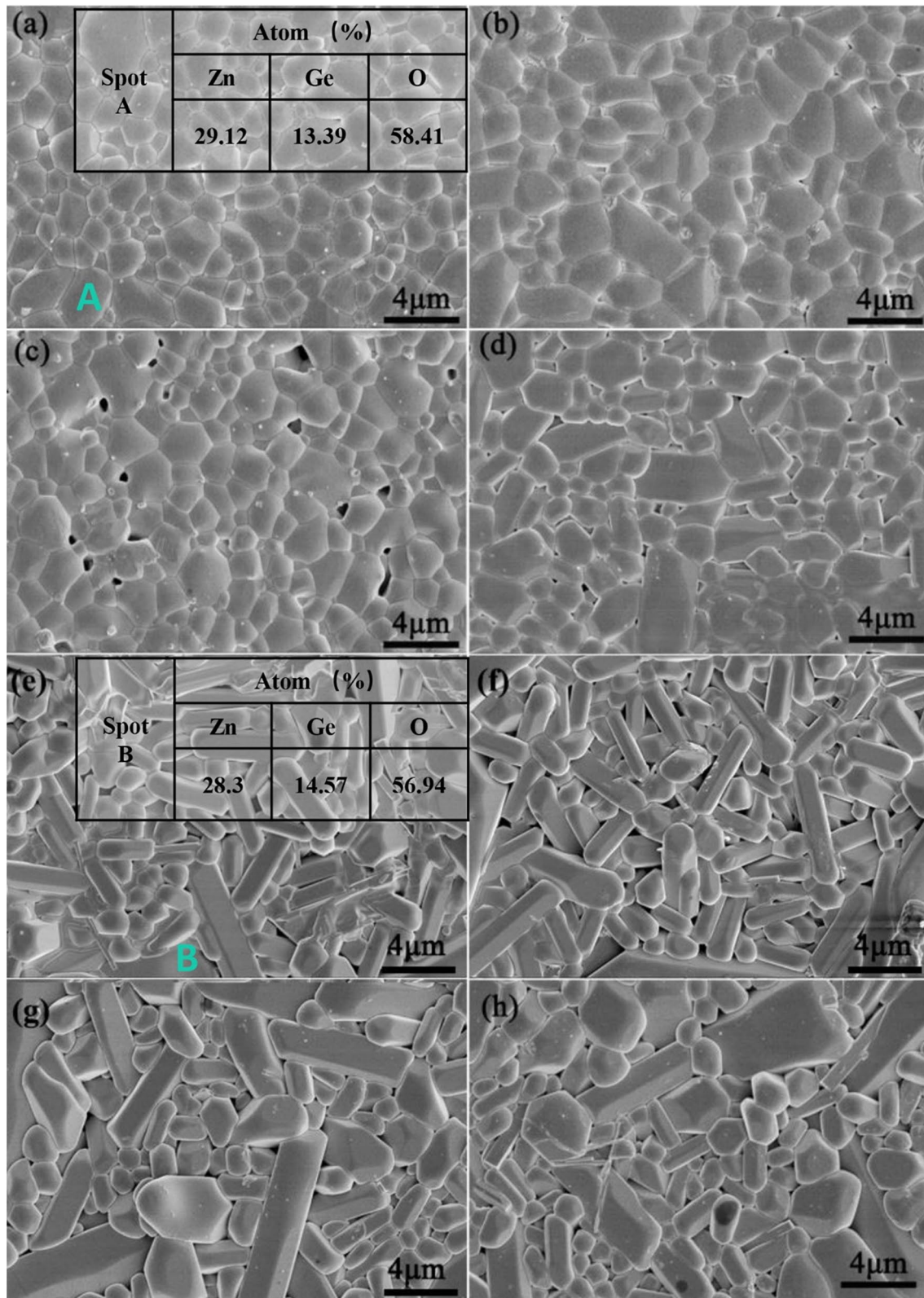


Fig. 3 SEM photographs of $\text{Zn}_2\text{Ge}_{1-x}\text{O}_{4+2x}$ ceramics sintered at their optimum temperatures for 6 h: **a** $x=-0.1$ at 1200 °C, **b** $x=-0.05$ at 1180 °C, **c** $x=0$ at 1160 °C, **d** $x=0.02$ at 1140 °C, **e** $x=0.05$ at 1080 °C, **f** $x=0.1$ at 1060 °C, **g** $x=0.15$ at 1040 °C and **h** $x=0.2$ at 1040 °C

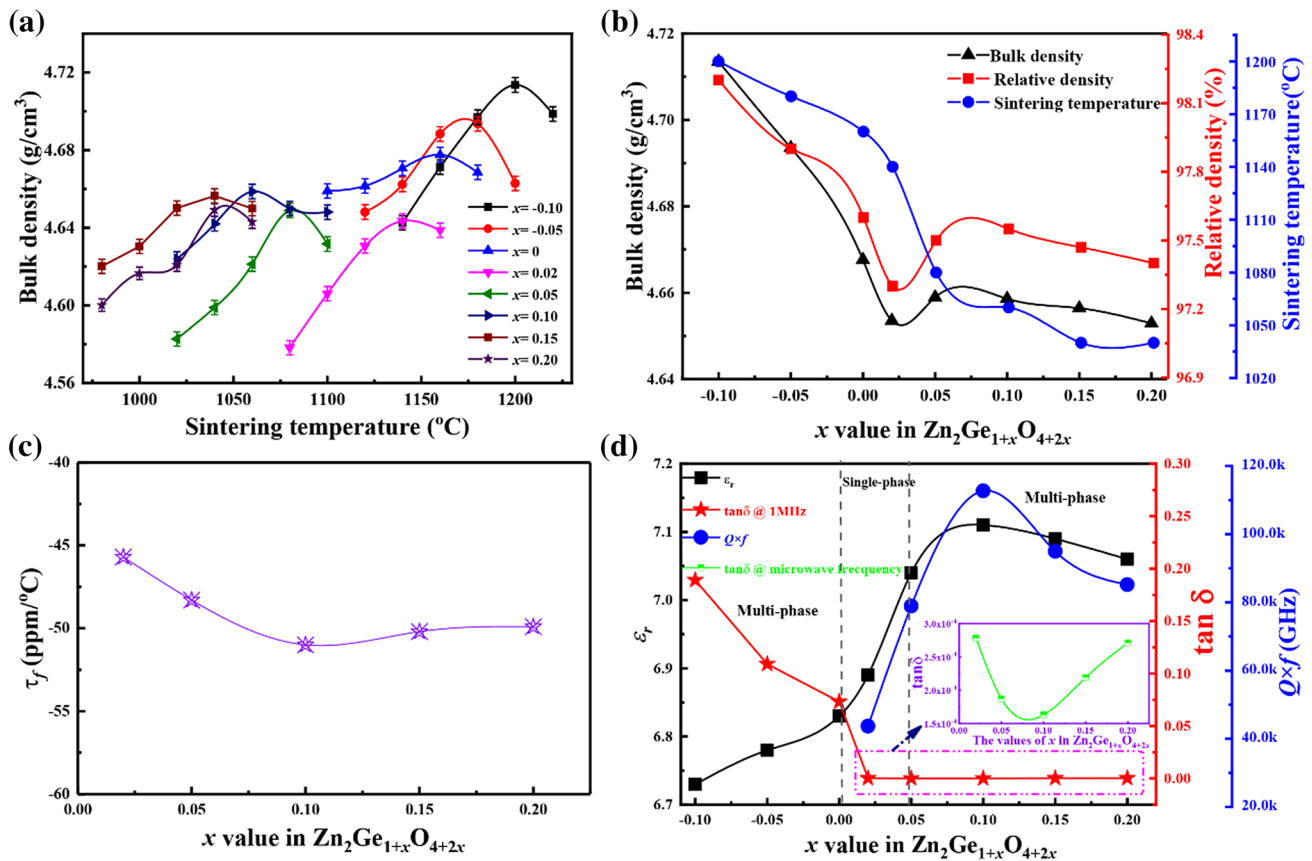


Fig. 4 The density and dielectric properties of $\text{Zn}_2\text{Ge}_{1+x}\text{O}_{4+2x}$ ($x = -0.1, -0.05, 0, 0.02, 0.05, 0.1, 0.15$ and 0.2)

as pores and grain boundaries, accounting for the increase in the quality factor, but excessive GeO_2 as the second phase would definitely generate dielectric loss and thus reduce the quality factor.

3.3 Raman and far-infrared reflection spectra

The room-temperature Raman spectra of $\text{Zn}_2\text{Ge}_{1+x}\text{O}_{4+2x}$ recorded in the range of 700 to 900 cm^{-1} are shown in Fig. 5a. Four Raman active modes were fitted by Lorentzian

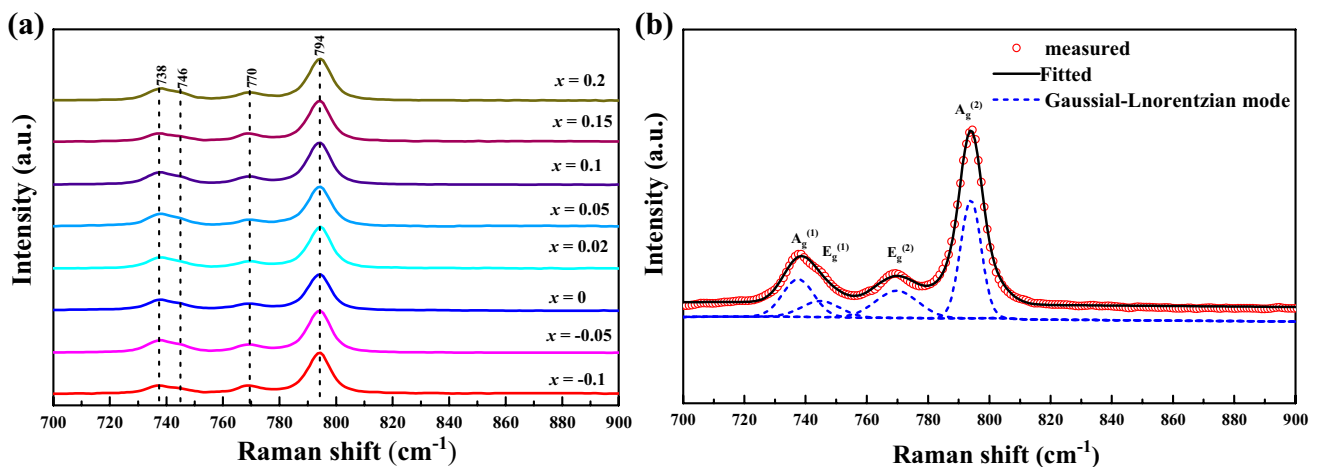


Fig. 5 **a** Raman spectra of $\text{Zn}_2\text{Ge}_{1+x}\text{O}_{4+2x}$ ($x = -0.1, -0.05, 0, 0.02, 0.05, 0.1, 0.15$ and 0.2) and **b** a typical fitting profile for $x = 0.1$

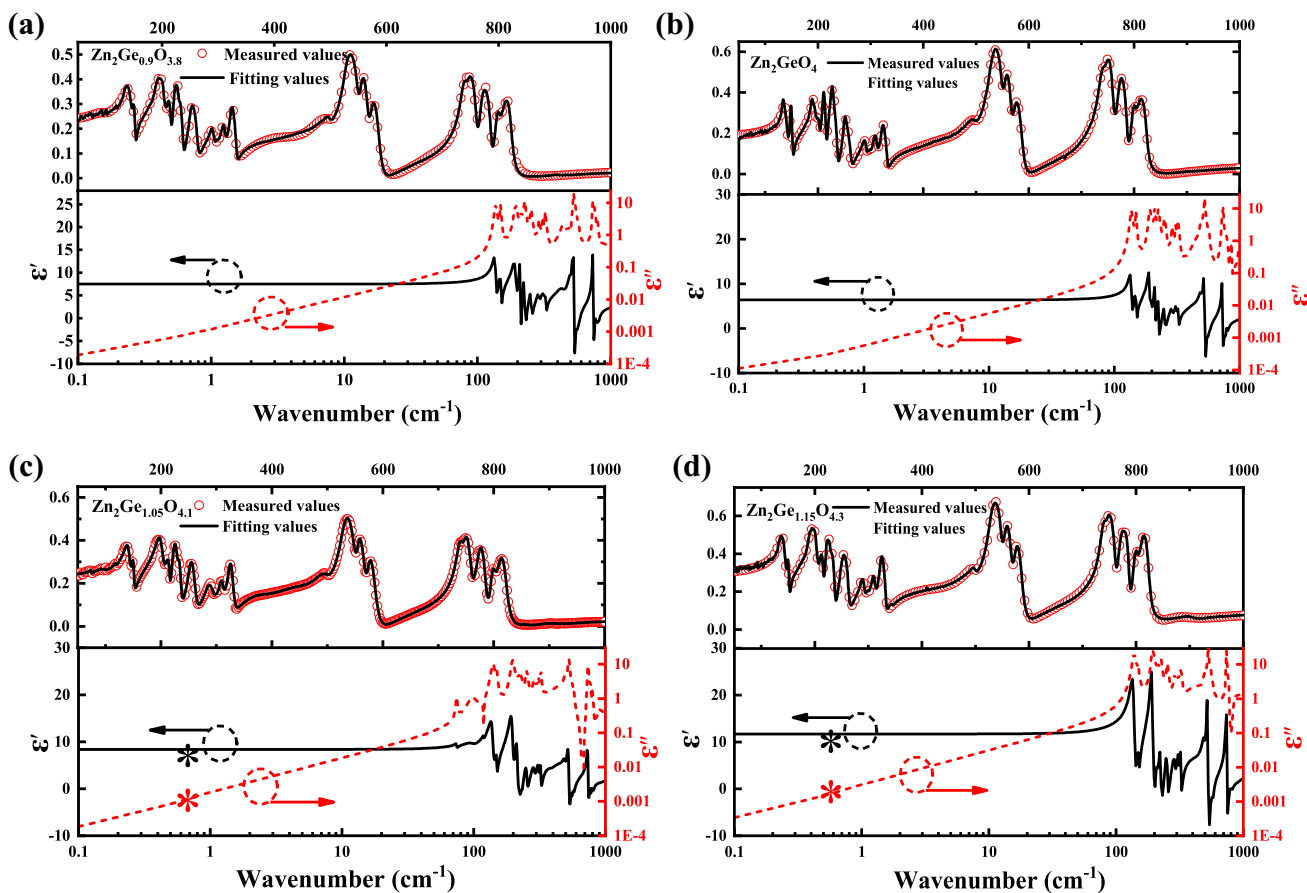


Fig. 6 Measured and calculated far-infrared reflectivity spectra and fitted complex dielectric spectra of $Zn_2Ge_{1+x}O_{4+2x}$ **a** $x = -0.1$; **b** $x = 0$; **c** $x = 0.05$; **d** $x = 0.15$

function, as shown in Fig. 5b. The strongest peak at 794 cm^{-1} is assigned to the stretching vibration of O–Ge–O in GeO_4 tetrahedra [21–23], while the Raman modes around 738 cm^{-1} and 769 cm^{-1} are attributed to the symmetric and asymmetric vibration of the external Ge–O–Zn, respectively [19, 24].

To obtain the intrinsic contributions of the dielectric properties, FIR spectra of the $Zn_2Ge_{1+x}O_{4+2x}$ were recorded and analyzed. The low-frequency modes between 200 and 400 cm^{-1} are related to Zn–O bend mode while those between 550 and 590 cm^{-1} correspond to Zn–O stretch mode [25]. The symmetric and anti-symmetric stretch modes of Ge–O tetrahedra locate at 700 – 900 cm^{-1} [26]. Based on the Kramers–Krönig analysis (K–K), the real part ϵ' and imaginary part ϵ'' of permittivity can be fitted by the following equations:

$$\epsilon'(\omega) = \epsilon_\infty + \sum_{j=1}^n \Delta\omega'_j = \epsilon_\infty + \sum_{j=1}^n \frac{\omega_{pj}^2}{\omega_{oj}^2} \tag{5}$$

$$\epsilon''(\omega) = \sum_{j=1}^n \frac{\gamma_j \omega_{pj}^2}{\omega_{oj}^2} \omega \tag{6}$$

The fitting results are shown in Fig. 6. The optical dielectric constant (ϵ_∞) is fitted as 0.8 – 0.95 , and the static value (ϵ_0) is 6.8 – 7.7 , which is close to the measured permittivity at the microwave frequency range. This result revealed that at microwave frequency region the dielectric response mainly stems from the absorptions of phonon oscillations. In contrast, all the fitted dielectric losses were lower than the measured ones using TE_{011} method. The theoretical quality factor of $Zn_2Ge_{1+x}O_{4+2x}$ ($x = -0.1, 0, 0.05, 0.15$) were fitted to be $198,753, 169,224, 215,234, 175,110$ GHz ($f = 14.48$ GHz), respectively. The deviation can be related to processing issues, e.g., the second phase, density, pore, and grain size. The fitting results indicate that there is still a wide space for dielectric properties optimization in the Zn_2GeO_4 system. Further efforts will be focused on processing optimization to minimize the extrinsic losses to further improve their $Q \times f$ values.

4 Conclusions

A series of $\text{Zn}_2\text{Ge}_{1+x}\text{O}_{4+2x}$ ceramics with $-0.1 \leq x \leq 0.2$, which were prepared by a simple solid-state reaction route, were investigated for microwave/millimeter-wave applications as low-permittivity substrates and Ge nonstoichiometry on the phase evolution and dielectric properties were studied in some details. Ge deficiency-induced ZnO as a second phase, whereas Ge excess favored the formation of single-phase willemite but a high level of excess induced appearance of GeO_2 . Ge excess was found beneficial to the densification and dielectric properties optimization. A composition $\text{Zn}_2\text{Ge}_{1.1}\text{O}_{4.2}$ with $x=0.1$ exhibited the optimum microwave dielectric properties with an $\epsilon_r \sim 7.09$, a $Q \times f \sim 112,700$ GHz (at 14.48 GHz), and $\tau_f \sim -51$ ppm/ $^\circ\text{C}$. Far-infrared spectra analysis reveal the optimum quality factor of Zn_2GeO_4 ceramics and offer the possibility to further improve their dielectric performances.

Acknowledgements This work was supported by Natural Science Foundation of China (Grant Nos. 21965009, 51502047, and 21761008), the Natural Science Foundation of Guangxi Zhuang Autonomous Region (Grant Nos. 2015GXNSFFA139003, 2016GXNSFBA380134, 2016GXNSFAA380018, and 2018GXNSFAA138175), and Project of Scientific Research and Technical Exploitation Program of Guilin (Grant No. 20170225). The authors would also like to thank the administrators in the IR beamline workstation of National Synchrotron Radiation Laboratory (NSRL) for their help in the IR measurement.

References

- M.T. Sebastian, R. Uvic, H. Jantunen, Low-loss dielectric ceramic materials and their properties. *Int. Mater. Rev.* **60**, 392–412 (2015)
- X.Q. Song, K. Du, J. Li, X.K. Lan, W.Z. Lu, X.H. Wang, W. Lei, Low-fired fluoride microwave dielectric ceramics with low dielectric loss. *Ceram. Int.* **45**, 279–286 (2019)
- C.C. Li, C.Z. Yin, J.Q. Chen, H.C. Xiang, Y. Tang, L. Fang, Crystal structure and dielectric properties of germanate melilites $\text{Ba}_2\text{MGe}_2\text{O}_7$ ($\text{M}=\text{Mg}$ and Zn) with low permittivity. *J. Eur. Ceram. Soc.* **38**, 5246–5251 (2018)
- Z.Y. Zou, X.K. Lan, W.Z. Lu, G.F. Fan, X.H. Wang, X.C. Wang, P. Fu, W. Lei, Novel high Curie temperature $\text{Ba}_2\text{ZnSi}_2\text{O}_7$ ferroelectrics with low-permittivity microwave dielectric properties. *Ceram. Int.* **42**, 16387–16391 (2016)
- X.Q. Song, K. Du, X.Z. Zhang, J. Li, W.Z. Lu, X.C. Wang, W. Lei, Crystal structure, phase composition and microwave dielectric properties of $\text{Ca}_3\text{MSi}_2\text{O}_9$ ceramics. *J. Alloys Compd.* **750**, 996–1002 (2018)
- H.C. Xiang, L. Fang, W.S. Fang, Y. Tang, C.C. Li, A novel low-firing microwave dielectric ceramic $\text{Li}_2\text{ZnGe}_3\text{O}_8$ with cubic spinel structure. *J. Eur. Ceram. Soc.* **37**, 625–629 (2017)
- D. Chen, F. Luo, D. Zhu, Dielectric and microwave absorption properties of divalent-doped $\text{Na}_3\text{Zr}_2\text{Si}_2\text{PO}_{12}$ ceramics. *J. Eur. Ceram. Soc.* **38**, 4440–4445 (2018)
- C.C. Li, Z.H. Wei, H. Luo, L. Fang, Sintering behavior and microwave dielectric properties of LiMVO_4 ($\text{M}=\text{Mg}$, Zn). *J. Mater. Sci.: Mater. Electron.* **26**, 9117–9121 (2015)
- D. Zhou, L.X. Pang, D.W. Wang, I.M. Reaney, BiVO_4 based high k microwave dielectric materials: a review. *J. Mater. Chem. C.* **6**, 9290–9313 (2018)
- C.C. Li, H.C. Xiang, M.Y. Xu, Y. Tang, L. Fang, Li_2AGeO_4 ($\text{A}=\text{Zn}$, Mg): two novel low permittivity microwave dielectric ceramics with olivine structure. *J. Eur. Ceram. Soc.* **38**, 1524–1528 (2018)
- J. Sugihara, K. Kakimoto, I. Kagomiya, H. Ohsato, Microwave dielectric properties of porous Mg_2SiO_4 filling with TiO_2 prepared by a liquid phase deposition process. *J. Eur. Ceram. Soc.* **27**, 3105–3108 (2007)
- N.H. Nguyen, J.B. Lim, S. Nahm, Effect of Zn/Si ratio on the microstructural and microwave dielectric properties of Zn_2SiO_4 ceramics. *J. Am. Ceram. Soc.* **90**, 3127–3130 (2007)
- C.X. Chen, S.P. Wu, Y.X. Fan, Synthesis and microwave dielectric properties of B_2O_3 -doped Mg_2GeO_4 ceramics. *J. Alloys Compd.* **578**, 153–156 (2013)
- S.P. Wu, Q. Ma, Synthesis, characterization and microwave dielectric properties of Zn_2GeO_4 ceramics. *J. Alloys Compd.* **567**, 40–46 (2013)
- Y.J. Eoh, E.S. Kim, High quality factor of $(\text{Zn}_{0.6}\text{Mg}_{0.4})_{1.918}\text{Ge}_{3.918}$ microwave dielectrics. *Ceram. Int.* **41**, S537–S543 (2015)
- B. Ma, F. Wen, H. Jiang, J. Yang, P. Ying, C. Li, The synergistic effects of two co-catalysts on Zn_2GeO_4 on photocatalytic water splitting. *Catal. Lett.* **134**, 78–86 (2010)
- X.H. Ma, S.H. Kweona, M. Imb, S. Nahm, Low-temperature sintering and microwave dielectric properties of B_2O_3 -added ZnO-deficient Zn_2GeO_4 ceramics for advanced substrate application. *J. Eur. Ceram. Soc.* **38**, 4682–4688 (2018)
- Q.S. Cao, W.Z. Lu, Z.Y. Zou, G.F. Fan, M. Fu, W. Lei, Phase compositions and reaction models of zinc manganese oxides with different Zn/Mn ratios. *J. Alloys Compd.* **661**, 196–200 (2016)
- V.B.R. Boppana, N.D. Hould, R.F. Lobo, Synthesis, characterization and photocatalytic properties of novel zinc germanate nanomaterials. *J. Solid State Chem.* **184**, 1054–1062 (2011)
- Y.X. Huang, Q.X. Cao, Z.M. Li, H.Q. Jiang, Y.P. Wang, G.F. Li, Effect of synthesis atmosphere on the microwave dielectric properties of ZnO powders. *J. Am. Ceram. Soc.* **92**, 2129–2131 (2009)
- Y.X. Zhao, S.W. Yang, J. Zhu, G.F. Ji, F. Peng, The study of oxygen ion motion in Zn_2GeO_4 by Raman spectroscopy. *Solid State Ion.* **274**, 12–16 (2015)
- S.K. Sharma, A.K. Misra, B. Sharma, Portable remote Raman system for monitoring hydrocarbon, gas hydrates and explosives in the environment. *Spectrochim. Acta A* **61**, 2404–2412 (2005)
- O. Yamaguchi, J. Hidaka, K. Hirota, Formation and characterization of alkoxy-derived Zn_2GeO_4 . *J. Mater. Sci. Lett.* **10**, 1471–1474 (1991)
- S.L. Zhang, F.M. Zeng, X.T. Wang, C. Li, C.W. Wang, Y. Zhang, H. Lin, J.M. Qin, J.H. Liu, Growth and structure characterization of Cr^{4+} doped Ca_2GeO_4 laser crystal. *Acta Phys Sin.* **59**, 7214–7218 (2010)
- C.W. Zheng, X.C. Fan, X.M. Chen, Analysis of infrared reflection spectra of $(\text{Mg}_{1-x}\text{Zn}_x)\text{Al}_2\text{O}_4$ microwave dielectric ceramics. *J. Am. Ceram. Soc.* **91**, 490–493 (2008)
- R. Jeanloz, Infrared spectra of olivine polymorphs: α , β phase and spinel. *Phys. Chem. Miner.* **5**, 327–341 (1980)

Publisher's Note Springer Nature remains neutral with regard to jurisdictional claims in published maps and institutional affiliations.